FRONTIERS OF PHYSICS

RESEARCH ARTICLE
Volume 21 / Issue 10 / 104201 / 2026

Computation simulation of stable perovskite solar cells with quasi-2D/2D bilayer for exceeding 30% efficiency

Guangdong Li, Mingxiang Xu†, Qingwang Bai

School of Physics, Southeast University, Nanjing 211189, China
Corresponding author. E-mail: †mxxu@seu.edu.cn
Received November 13, 2025; accepted January 9, 2026

ABSTRACT

Layered quasi-two-dimensional (quasi-2D)/2D perovskites have attracted enormous interest in photovoltaics owing to their promising optical properties and superior long-term structural stability. This study presents a novel design of perovskite solar cells (PSCs) with a quasi-2D/2D bilayer configuration (FTO/NiO/$(BA)_2MASn_2I_7$/$NH_3(CH_2)_2NH_3MnCl_4$/BiI_3/Au), which was numerically investigated using the wxAMPS simulator for the first time. Wherein, the quasi-2D $(BA)_2MASn_2I_7$ with an organic spacer, serving as the light harvester, exhibits appealing stability and carrier mobility, while the 2D $NH_3(CH_2)_2NH_3MnCl_4$ acts as a capping layer that mitigates the degradation of the underlying quasi-2D perovskite. The simulation results reveal that the quasi-2D/2D structure can facilitate the efficient diffusion and transport of charge carriers to the corresponding electrodes and suppress the defect state density and carrier recombination, benefiting from the gently stepped energy band structure. Additionally, this study analyzes the effects of the thickness of each absorber layer, the doping concentration of the $NH_3(CH_2)_2NH_3MnCl_4$ layer, and the interfacial layer materials on the performance parameters of PSCs. We found that the thickness of $(BA)_2MASn_2I_7$ has a positive impact on the short-circuit current density (J_{sc}) and fill factor (FF) of the device, whereas the thickness of $NH_3(CH_2)_2NH_3MnCl_4$ significantly degrades the photoelectric parameters of the solar cells. A moderate doping concentration (3.2×10^{14} cm^{-3}) in the $NH_3(CH_2)_2NH_3MnCl_4$ layer can effectively reduce carrier recombination within the PSCs. Finally, the optimal-performance PSCs based on the quasi-2D/2D structure achieve a power conversion efficiency (PCE) of 30.09% when using an $In_2(O, S)_3$ interfacial layer, which yields a lower series resistance (R_s). This work provides a novel strategy for realizing PSCs with both high photovoltaic performance and excellent stability.

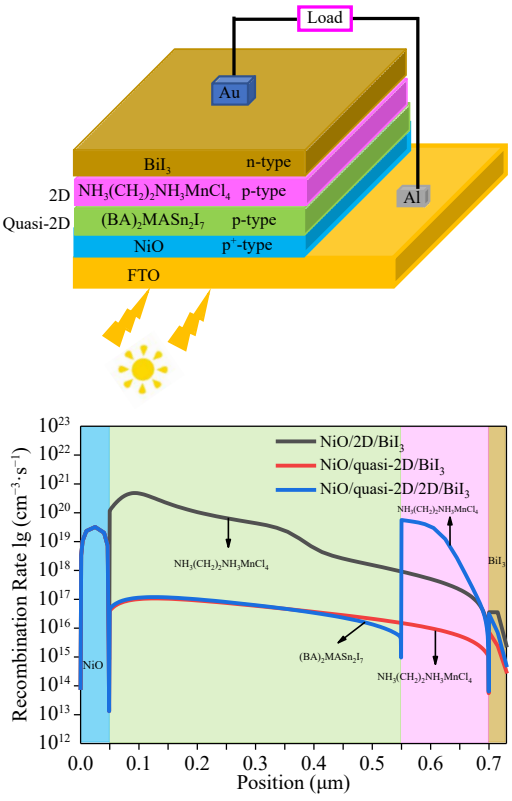

Keywords quasi-2D/2D bilayer PSCs, stability, capping layer, diffusion motion, transmission of charge carriers, optimum-performance

1 Introduction

The organometal halide bulk three-dimensional (3D) perovskite solar cells (PSCs) have garnered considerable attention in the photovoltaic community over the last decade, owing to their notable optoelectronic properties, including a high extinction coefficient, facile fabrication processability, and rapidly growing power conversion efficiency (PCE) [1–5]. The single-junction bulk PSCs have achieved a record PCE, increasing from the original 3.8% to over 26% [6–10]. However, the poor stability

https://doi.org/10.15302/frontphys.2026.104201

and photochemical reactions of 3D perovskite materials give rise to rapid degradation, which has been a barrier to the prospect of commercialization [11]. Hence, to overcome this drawback, researchers have already focused on various experimental and theoretical studies to improve the stability of PSCs, yielding promising results, such as perovskite composition engineering, interfacial regulation, defect passivation, and the processing of additives, among others [12–15]. Inspired by the aforementioned research tactics, low-dimensional quasi-two-dimensional (quasi-2D) or two-dimensional (2D) perovskites, protected by periodic organic ligands, not only exhibit facile film surface formation and solvable processing but also display excellent optoelectronic properties and superior chemical and thermal stability [16–18]. They have been used as absorber layers in the preparation of PSCs. This is attributed to the fact that hydrophobic long-chain organic cations can be incorporated by quasi-2D or 2D perovskites, effectively preventing the permeation of moisture in the perovskite lattice [19–21]. In addition, the optical properties of 2D perovskites have also received numerous research focuses thanks to the strong quantum and dielectric confinement effects [22]. In 2014, the $(PEA)_2(MA)_2Pb_3I_{10}$ quasi-2D PSCs were first reported by Karunadasa *et al.* [23] with a PCE of 4.73%. Zuo *et al.* [24] presented the simple drop-casting method for preparing hybrid perovskite films comprising both quasi-2D and quasi-3D phases, and an enhanced PCE of 16.0% was achieved using an iso-butylammonium-based quasi-2D/3D perovskite layer in 2020. Hailegnaw *et al.* [25] reported quasi-2D p-i-n PSCs incorporating alpha-methylbenzyl ammonium iodide (MBAI) cations, which achieved a certified PCE in the range of 15% and demonstrated outstanding operational stability in 2023. Additionally, in 2019, Zuo *et al.* [26] prepared uniform and highly oriented 2D-perovskite films using the drop-casting method, yielding PSCs with a PCE of up to 14.9%. Yan *et al.* [27] fabricated a photodetector based on Ruddlesden-Popper perovskite microwires photodetector possessed a wider photoresponse range and higher responsivities of 233 A/W in the visible band and 30 A/W in the near-infrared band in 2023. Zhang *et al.* [28] demonstrated ultrastable and efficient 2D Dion–Jacobson (DJ) PSCs and achieved a maximum stabilized PCE of 19.11% under an environmental atmosphere in 2024. Nevertheless, most of the reported PCE of single junction quasi-2D and 2D PSCs hardly exceed 20%. This is attributed to the fact that most perovskites with a monolayer quasi-2D or 2D crystal structure cannot be sufficiently absorbed by different wavelengths of light, which hinders charge transport due to the heterogeneous distribution of spacer layers with organic cations [29]. Therefore, it is a momentous frontier field to explore a novel approach to improve the photoelectric performance of quasi-2D and 2D PSCs while maintaining stability. In 2025, Banerjee *et al.* [30] constructed 2D $(A43)_2PbI_4$ (A43: $(CF_3)_3CO(CH_2)_3NH_3^+$)/quasi-2D $(A43)_2MAPb_2I_7$ heterojunction perovskites and achieved a high-efficiency device with 32% efficiency through theoretical calculations. However, such perovskite layers still contain toxic lead elements, which pose a serious threat to the environment.

Excitingly, the quasi-2D perovskite $(BA)_2MASn_2I_7$ ($(C_4H_9NH_3)_2CH_3NH_3Sn_2I_7$) can exhibit high carrier mobility and non-toxic characteristic, thus it may be possible to improve the charge carriers transport and optoelectronic properties in the PSCs [31]. To our knowledge, few review articles can be identified on $(BA)_2MASn_2I_7$ by reason of complex calculations in photovoltaic devices [32]. Therefore, it is much significative and necessary to research the effect of the $(BA)_2MASn_2I_7$ material on the photoelectric properties of PSCs. Moreover, the intermediate dimension-based perovskites with dissimilar layered quasi-2D or 2D perovskites with other layered perovskite materials incorporate distinct heterostructures that appear to display unique optical and optoelectronic properties [32]. Nevertheless, there are few reports regarding the excellent photoelectric properties of intermediate dimension-based dual layered quasi-2D/2D perovskites for photovoltaic, focusing on 2D/3D perovskites or 2D/3D/2D perovskites or without including the latest results. Additionally, the 2D $NH_3(CH_2)_2NH_3MnCl_4$ has also high resistivity to moisture and eco-friendliness, and behaves as a capping layer that mitigates the degradation of the underlying quasi-2D perovskite in the quasi-2D/2D perovskite structure [33]. Consequently, the quasi-2D/2D perovskites ($(BA)_2MASn_2I_7$/$NH_3(CH_2)_2NH_3MnCl_4$) are regarded as a possible option to improve the stability and performance of the photovoltaic device.

In this work, the new structural quasi-2D/2D bilayer PSC (FTO/NiO/$(BA)_2MASn_2I_7$/$NH_3(CH_2)_2NH_3MnCl_4$/BiI_3/Au) was numerically calculated and reported. Since $(BA)_2MASn_2I_7$ and $NH_3(CH_2)_2NH_3MnCl_4$ have similar layered perovskite structure, the $NH_3(CH_2)_2NH_3MnCl_4$ as a capping layer growing on $(BA)_2MASn_2I_7$ passivates the grain boundaries of $(BA)_2MASn_2I_7$ perovskite, which is likely to derive high quality films with minor defects. The simulation revealed that the quasi-2D/2D structure can facilitate the efficient diffusion motion and transmission of charge carriers to the corresponding electrode. Moreover, the effects of the thickness parameters of each absorber layer, the doping concentration of the $NH_3(CH_2)_2NH_3MnCl_4$ layer, and the interfacial layer materials on the photoelectric characteristics of PSCs are analyzed and compared by numerical simulation. The results display the optimal-performance (30.09%) for the PSCs with the quasi-2D/2D structure.

2 Simulated device configurations

To contrast and investigate the effects of different device configurations on the photoelectric characteristic of

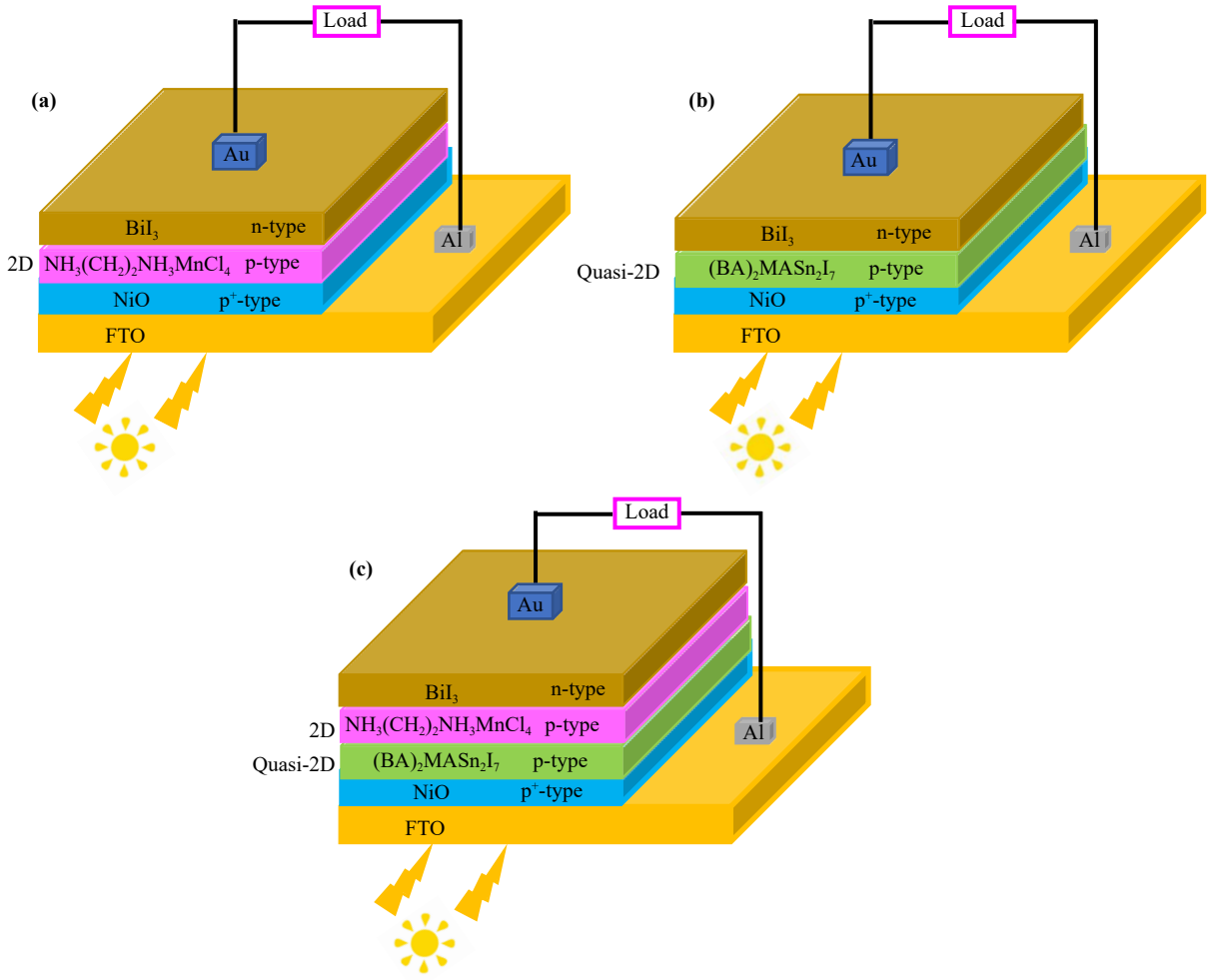

Fig. 1 The schematic architecture of **(a)** $NH_3(CH_2)_2NH_3MnCl_4$ based PSC, **(b)** $(BA)_2MASn_2I_7$ based, and **(c)** $(BA)_2MASn_2I_7/NH_3(CH_2)_2NH_3MnCl_4$ based PSC.

PSCs, the numerical modeling has been carried out through employing wxAMPS simulator under the illumination condition of AM 1.5G solar spectrum and operating temperature of 300 K. The three device architectures are depicted in Figs. 1(a–c), respectively, FTO/NiO/$NH_3(CH_2)_2NH_3MnCl_4$/BiI_3/Au (Device1), FTO/NiO/$(BA)_2MASn_2I_7$/BiI_3/Au (Device2) and FTO/NiO/$(BA)_2MASn_2I_7/NH_3(CH_2)_2NH_3MnCl_4/BiI_3$/Au (Device3). The tunneling effect was considered in the wxAMPS model by setting trap-assisted tunneling models and intra-band tunneling. The wxAMPS software can simulate that when the active material of perovskite solar cells is exposed to light, the photons with energy greater than the material's band gap will excite electrons to transition from the valence band to the conduction band, leaving holes in the valence band and forming photogeneration electron–hole pairs (excitons). These excitons dissociate into free carriers (free electrons and holes) under the action of thermal energy, and then are separated and transported to the electrodes by the internal electric field, forming the photogenerated current. Under short-circuit conditions, the electron flux (photogenerated current) is defined by the interplay of exciton photogeneration in the active layer, geminate and non-geminate recombination processes, and free charge carriers' extraction [34]. The performance parameters and photophysical parameters (such as electric field intensity and distribution, energy band structure, photogenerated carrier concentration, and J–V characteristic curve) of the device can be extracted to solve the fundamental semiconductor device equations (Poisson's equation, hole-electron continuity equations) under one-dimensional conditions through iterative method, and then solving for the vacuum energy levels and hole-electron quasi-fermi levels at various positions within the solar cell [35, 36]. For the proposed device configurations, the transparent conduction oxide (FTO) and Au are used as the front contact electrode and back contact electrode. NiO (50 nm) and BiI_3 (30 nm) are utilized as the hole transport layer (HTL) and interfacial layer, respectively. The $(BA)_2MASn_2I_7$ (500 nm) and $NH_3(CH_2)_2NH_3MnCl_4$ (150 nm) are all acted as light absorption layers.

Table 1 Material parameters of the simulated PSCs.

Parameters	NiO [37, 38]	$(BA)_2MASn_2I_7$ [31, 39]	$NH_3(CH_2)_2NH_3MnCl_4$ [33, 40]	BiI_3 [41–45]
Thickness (nm)	50	500	150	30
Relative permittivity ε_r	11.75	5.44	6	5.78
Electron affinity χ (eV)	2.1	3.5	4.17	4.10
Band gap E_g (eV)	3.6	1.554	1.8	1.72
Effective conduction band density N_c (cm^{-3})	2.5×10^{20}	–	1×10^{18}	2.5×10^{19}
Effective valence band density N_v (cm^{-3})	2.5×10^{20}	–	1×10^{19}	2.5×10^{19}
Electron mobility μ_n ($cm^2\cdot V^{-1}\cdot s^{-1}$)	1×10^{-3}	168.5	1.6	600
Hole mobility μ_p ($cm^2\cdot V^{-1}\cdot s^{-1}$)	1×10^{-3}	255	1.6	200
Acceptor density N_A (cm^{-3})	1×10^{19}	0	3.2×10^{15}	1×10^{16}
Donor density N_D (cm^{-3})	0	0	0	1×10^{16}
Defect density N_t (cm^{-3})	1×10^{14}	1×10^{14}	1×10^{14}	1×10^{14}

Wherein the thicknesses of the single layer $NH_3(CH_2)_2NH_3MnCl_4$ absorber layer [Fig. 1(a)], the $(BA)_2MASn_2I_7$ absorber layer [Fig. 1(b)] as well as the bilayer $(BA)_2MASn_2I_7/NH_3(CH_2)_2NH_3MnCl_4$ absorber layers [Fig. 1(c)] were all set to 650 nm. The transport mechanism of the photogenerated carriers within PSCs can be as follows: the electron transmission from the conduction band of the perovskite absorber layer to the Au back contact electrode via the BiI_3 interfacial layer, while the hole gets transferred from the valence band of the perovskite absorber layer to the FTO front contact electrode via the NiO HTL. The schematic architectures of the PSCs with the $NH_3(CH_2)_2NH_3MnCl_4$, $(BA)_2MASn_2I_7$, and $(BA)_2MASn_2I_7/NH_3(CH_2)_2NH_3MnCl_4$ as their respective absorber layers are depicted in Figs. 1(a)–(c), respectively. The input material parameters of the three configurations involved in our simulations are summarized in Table 1 [31, 33, 37–45]. Regarding the defect densities presented in Table 1, taking the report in this literature as an example [46], we found that the interface trap density at the interface of the perovskite layer is relatively high (1×10^{17} cm^{-3}), while the bulk trap density of the perovskite layer is inferior (5×10^{14} cm^{-3}). Since the defects at the interface are not considered in this work, the defect density of each functional layer is set to the order of 10^{14} cm^{-3}. Additionally, based on the tests of the absorption spectra of $NH_3(CH_2)_2NH_3MnCl_4$ and $(BA)_2MASn_2I_7$ materials in relevant literature, the $NH_3(CH_2)_2NH_3MnCl_4$ and $(BA)_2MASn_2I_7$ exhibit the rough absorption edge at 685 nm and 814 nm, respectively [47, 48]. Therefore, both of these materials can absorb visible light within a relatively long wavelength range.

3 Results and discussion

The J–V characteristics curves of the $NH_3(CH_2)_2NH_3MnCl_4$ (2D), $(BA)_2MASn_2I_7$ (quasi-2D), and $(BA)_2MASn_2I_7/NH_3(CH_2)_2NH_3MnCl_4$ (quasi-2D/2D) separately as the light absorption layer PSCs are displayed in Fig. 2(a). Table 2 presents the comparisons of the detailed PSCs performance parameters acquired from our simulation. The conspicuous detections in Fig. 2(a) and Table 2 bespeak that short-circuit current density (J_{sc}) and open-circuit voltage (V_{oc}) increase from 16.76 mA/cm^2 and 0.90 V for the 2D absorber layer PSC to 24.97 mA/cm^2 and 1.17 V for the quasi-2D/2D absorber layer structure, respectively. This significant increment in performance parameters can be related to the narrower band gap of $(BA)_2MASn_2I_7$ and quasi-2D/2D structure, which modulates the band alignment at the interfaces of each functional layer and brings about the extended photogeneration in a broad range of photon spectrum. In addition, the 2D perovskite layer with a wider band gap placed above the quasi-2D perovskite layer with a narrower band gap can fully absorb short-wavelength light, enhancing the absorption rate of the entire solar spectrum. This enables greater utilization of solar energy to generate more photogeneration carriers, thereby achieving the higher J_{sc} [49]. Contrast of the J–V curves proclaims that albeit the J_{sc} and V_{oc} of the quasi-2D/2D structure are marginally lower than those of the quasi-2D absorber layer device, the quasi-2D/2D device manifests better PCE due to its higher fill factor (FF).

The energy band diagrams of PSCs with different configurations are illustrated in Figs. 2(b)–(d) (under the illumination condition of AM 1.5G solar spectrum and applied voltage of –0.3 V) and Figs. 3(a)–(c) (under the dark condition and without bias), respectively. As established in Fig. 3, the barrier height (qV_{bi}) of the p–n junction can be defined by the conduction band energy level difference of the light absorption layer at the interfaces of NiO/absorber and absorber/BiI_3. The built-in potential (V_{bi}) is an equilibrium property that is obtained in the dark and without bias [50]. The value of V_{bi} in the energy band diagrams can be estimated by the difference between the conduction bands on both sides of the interface between the absorber and transport layers divided by

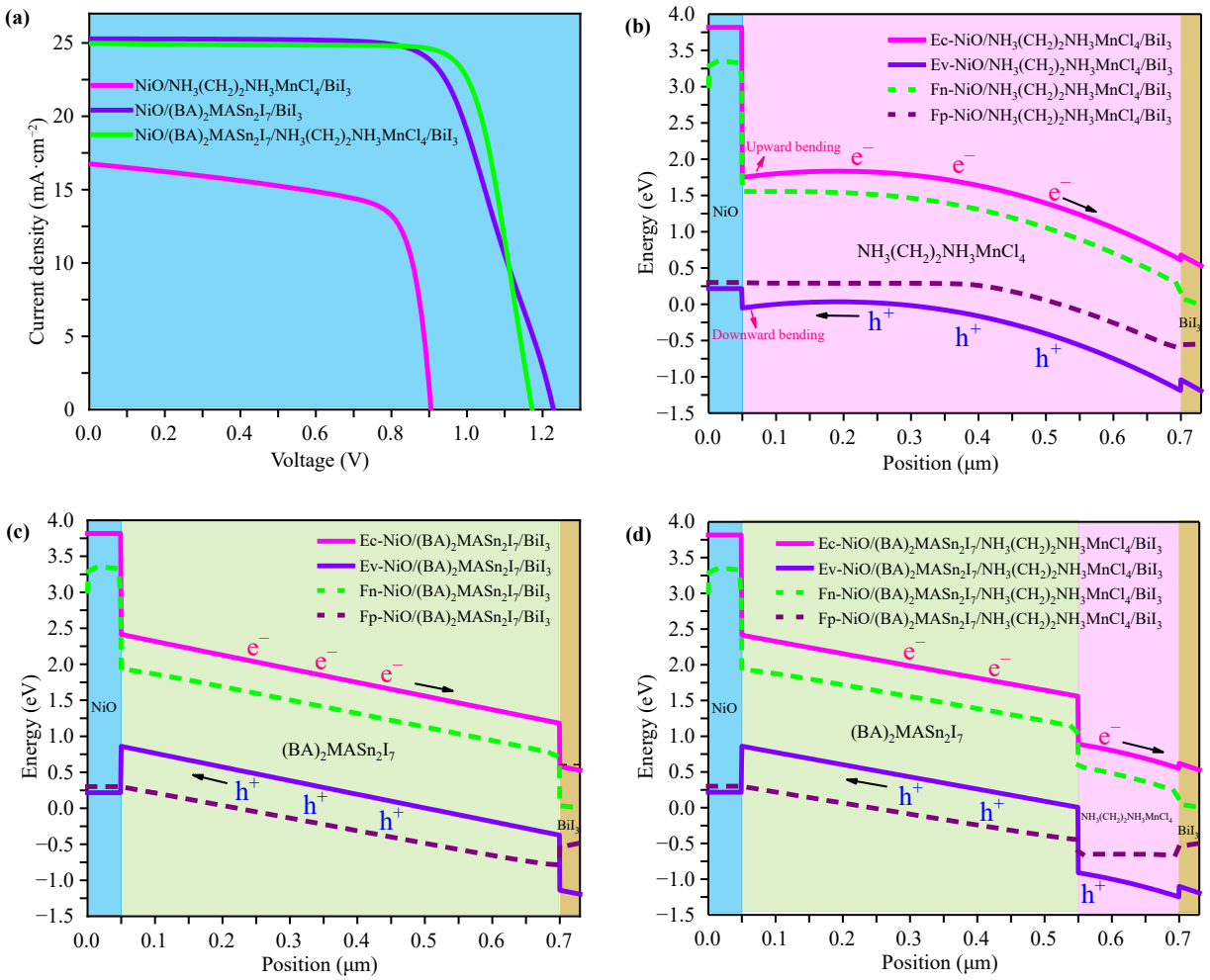

Fig. 2 **(a)** The J–V characteristics curves and **(b–d)** energy band diagrams of three PSC configurations (under the illumination condition of AM 1.5G solar spectrum and applied voltage of –0.3 V).

Table 2 Comparisons of the performance parameters of the PSCs with different configurations.

Device configurations	V_{oc} (V)	J_{sc} (mA·cm^{-2})	FF (%)	PCE (%)
FTO/NiO/$NH_3(CH_2)_2NH_3MnCl_4$/BiI_3/Au	0.90	16.76	70.33	10.67
FTO/NiO/$(BA)_2MASn_2I_7$/BiI_3/Au	1.23	25.28	69.25	21.51
FTO/NiO/$(BA)_2MASn_2I_7$/$NH_3(CH_2)_2NH_3MnCl_4$/ BiI_3/Au	1.17	24.97	78.58	23.01

the elementary charge q [51]. Therefore, the V_{bi} is the qV_{bi} divided by the elementary charge q (q = 1.602×10^{-19} C ≈ 1 eV), they are 0.79 V, 1.55 V, and 1.51 V for 2D, quasi-2D, and quasi-2D/2D absorber layer PSCs, respectively. The larger V_{bi} can effectively reduce the separation and migration of carriers [52], therefore, the highest and lowest V_{oc} (1.23 V and 0.90 V) correspond to the quasi-2D and 2D absorber layer PSCs, respectively. Furthermore, the large conduction band offset between the NiO HTL and the absorber layer, effectively prohibiting the electrons at the HTL. Meanwhile, the study found that in Fig. 2(b), the energy band curves of the PSCs based on the 2D absorber layer show an upward bending. This not only directly leads to the reduction in V_{bi}, but also results in the electron energy at the ordinate near the NiO/$NH_3(CH_2)_2NH_3MnCl_4$ interface being lower than that in the $NH_3(CH_2)_2NH_3MnCl_4$ absorber layer, which will seriously hinder the transport and extraction of charge carriers to the electrode. Therefore, the performance of the device is relatively poor. In Fig. 2(d), the most worth noting that the quasi-2D/2D dual absorber layer designed in this study features a gentle stepped energy band structure, and there's no bending of the energy band. This structure reduces the band offset at the $NH_3(CH_2)_2NH_3MnCl_4$/BiI_3 interface, effectively minimiz-

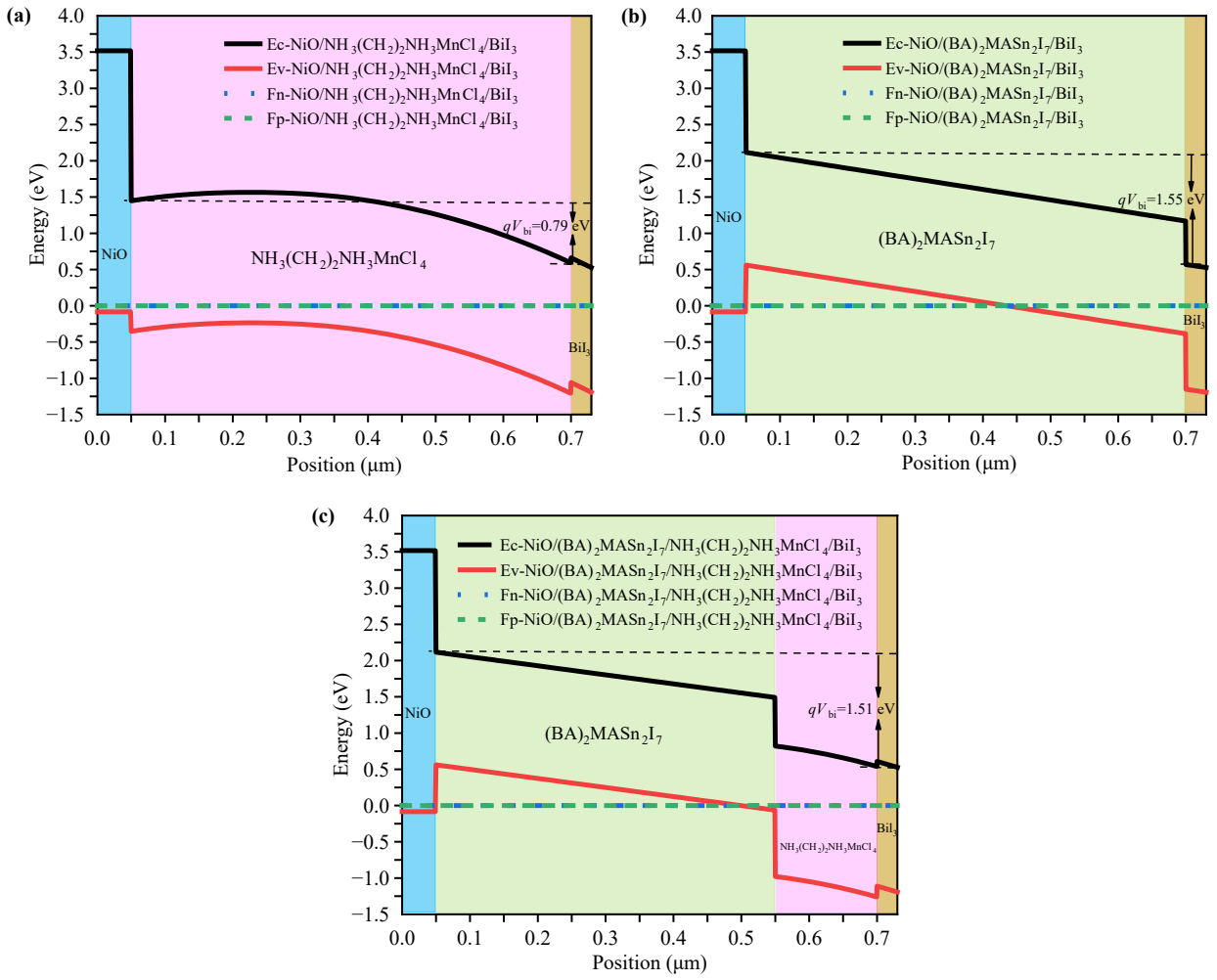

Fig. 3 **(a–c)** The energy band diagrams of three PSC configurations (under the dark condition and without bias).

ing the energy loss required for electron diffusion at the interface of $NH_3(CH_2)_2NH_3MnCl_4/BiI_3$, while being more conducive to improving the transport and extraction efficiency of charge carriers. Additionally, despite the relatively large valence band barrier at the $NiO/(BA)_2MASn_2I_7$ interface can impede the drift motion of holes, but the greater electron and hole concentration differences appear at the interface of $NiO/(BA)_2MASn_2I_7$ [Fig. 4(a)] and lower carrier recombination at the $NiO/(BA)_2MASn_2I_7$ interface of the quasi-2D/2D PSCs [Fig. 4(c)]. Therefore, more holes in the $(BA)_2MASn_2I_7$ absorber layer can be transported and extracted to the NiO layer through diffusion motions at the interface of $NiO/(BA)_2MASn_2I_7$. Moreover, we also hypothesize that holes can also pass through the barrier via quantum tunneling due to the thin NiO HTL (Hence the high J_{sc} (24.97 $mA \cdot cm^{-2}$, Table 2) was generated). Consequently, this quasi-2D/2D structure can effectively improve the FF and PCE of the PSCs [53, 54].

Further calculations on the carrier concentration distributions of the proposed PSCs with different configurations indicate that the quasi-2D/2D structure yields higher electron concentration near the interface of $NH_3(CH_2)_2NH_3MnCl_4/BiI_3$, as shown in Fig. 4(a), which means that more electrons can be transported to the Au back contact electrode. Additionally, the greater electron and hole concentration differences appear at the interfaces of each functional layer in the quasi-2D/2D structure. The large carrier concentration differences will be more conducive to the diffusion motions of the carriers, effectively improving the mobility of the carriers. As can be observed from the current density distributions of the three configurations of PSCs in Fig. 4(b) that the total current density of the quasi-2D/2D PSCs is slightly lower than that of the quasi-2D PSCs, which matches the J_{sc} of the quasi-2D/2D PSCs being marginally below that of the quasi-2D PSCs in Fig. 2(a). The calculated recombination rates in different layers of the three configurations are presented in Fig. 4(c). It can be seen that although the recombination rate of the quasi-2D/2D PSCs in the $(BA)_2MASn_2I_7$ layer is mildly lower than that of the quasi-2D PSCs, the more recombination in the $NH_3(CH_2)_2NH_3MnCl_4$ layer (0.55–0.7 μm) of the

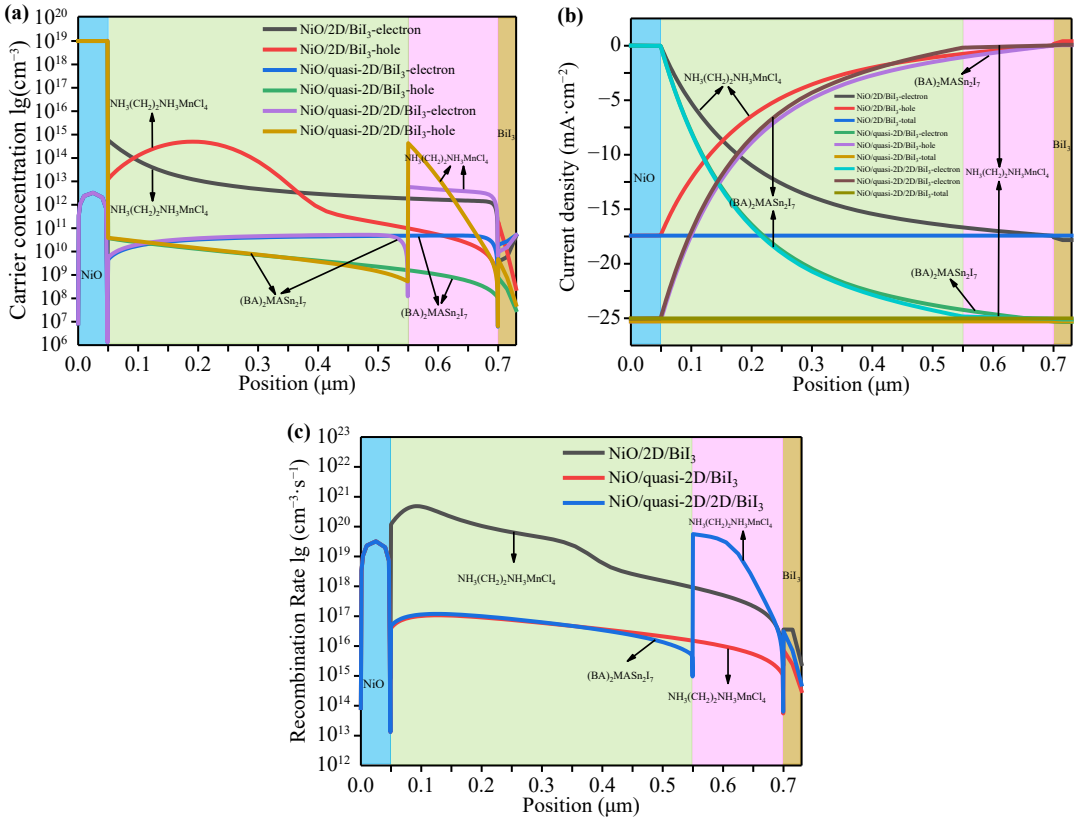

Fig. 4 **(a)** The carrier concentration distributions, **(b)** current density distributions, and **(c)** recombination rate diagrams of the PSCs with three device configurations (under the illumination condition of AM 1.5G solar spectrum and applied voltage of –0.3 V).

quasi-2D/2D PSCs compared to the other two structures of the PSCs. Accordingly, some parameters in the $NH_3(CH_2)_2NH_3MnCl_4$ layer need to be further optimized to elevate device performance.

The thickness of the absorber layer is a decisive factor will directly affect the generation of excitons and carrier separation, which is the dominant factor in determining the performance of the PSCs [35, 55]. The effect of quasi-2D $(BA)_2MASn_2I_7$ absorber layer thickness on the performance parameters and PCE of the quasi-2D/2D structure device with the assessment range from 300 nm to 700 nm is presented in Figs. 5(a) and (b). Among the simulated results, the device performance parameters (J_{sc}, FF, and PCE) barring V_{oc} are enhanced evident with the expansion of $(BA)_2MASn_2I_7$ thickness. The J_{sc} is steadily improved from 24.04 mA/cm^2 to 25.31 mA/cm^2 with the $(BA)_2MASn_2I_7$ thickness enlarging from 300 nm to 700 nm. This is attributed to the evidently enhanced photon absorption under the larger absorber layer thickness. Nevertheless, the FF and PCE decrease marginally as the $(BA)_2MASn_2I_7$ thickness exceeds 600 nm, which due to the too large $(BA)_2MASn_2I_7$ thickness may cause an enormous boost in the charge carriers recombination rates and higher series resistance. Furthermore, as can be observed in Fig. 5(c), the energy level gap is gradually expanded with the increase of the $(BA)_2MASn_2I_7$ thickness. The excessively large energy level gap increases the energy loss required for carriers' diffusion at the $(BA)_2MASn_2I_7/NH_3(CH_2)_2NH_3MnCl_4$ interface, as well as the recombination loss of carriers, resulting in the loss of V_{oc}. Accordingly, the V_{oc} drops gradually as the increasing $(BA)_2MASn_2I_7$ thickness in Fig. 5(a). The highest PCE (23.12%) is attained when the optimum thickness (600 nm) is used in our simulation study.

The effect of the 2D $NH_3(CH_2)_2NH_3MnCl_4$ absorber layer thickness on the quasi-2D/2D structure PSCs performance parameters and PCE are computationally simulated by executing J–V analysis, as shown in Figs. 5(d) and (e). The performance parameters are all getting worse as the $NH_3(CH_2)_2NH_3MnCl_4$ absorber layer thickness increases. It is well known that the carriers inside 2D perovskite have shorter diffusion lengths and lower mobilities compared to 3D perovskite [21]. Therefore, the thicker $NH_3(CH_2)_2NH_3MnCl_4$ absorber layer will increase the carrier recombination probability to a large extent, this can also be verified from the calculated recombination rate curves in Fig. 5(f), and hence the PCE of the device declines profoundly. Additionally, the high stability 2D perovskite layer can be also behaved as

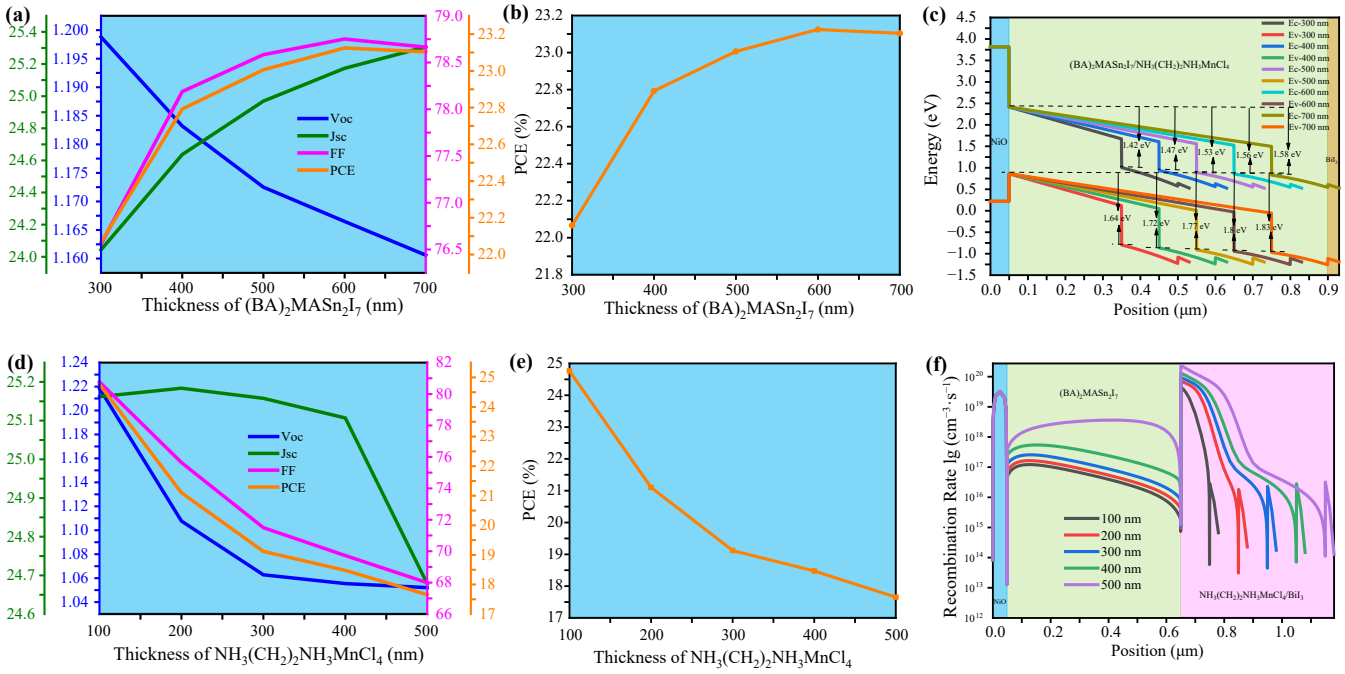

Fig. 5 Effect of quasi-2D $(BA)_2MASn_2I_7$ absorber layer thickness on the **(a)** device performance parameters, **(b)** PCE, **(c)** energy band diagrams, and 2D $NH_3(CH_2)_2NH_3MnCl_4$ absorber layer thickness on the **(d)** device performance parameters, **(e)** PCE and **(f)** recombination rate curves (under the illumination condition of AM 1.5G solar spectrum and applied voltage of –0.3 V).

a capping layer to avoid the degradation of the bottom perovskite layer and elevate the stability of the entire quasi-2D/2D structure PSCs [20]. In our proposed structure, the optimal PCE (24.77%) is derived when the smaller thickness of the $NH_3(CH_2)_2NH_3MnCl_4$ absorber layer is 100 nm.

The doping concentration refers to the number density of impurity atoms doped into perovskite materials, and it is a momentous parameter for regulating the conductivity type (n-type/p-type) and carrier concentration of perovskite materials. Additionally, the doping concentration can directly affect the photoelectronic properties of PSCs, such as V_{bi}, carriers' generation and recombination [56, 57]. The simulation study on doping concentration is equivalent to changing the carrier concentration by introducing impurity atoms or defects (bulk doping), and altering the separation and transport efficiency of charge carriers by regulating the position of the conduction band bottom or valence band top of the material. Accordingly, comprehending the doping physical perception is exceedingly prominent in the fabrication of efficient PSCs. Figures 6(a) and (b) present the impact of $NH_3(CH_2)_2NH_3MnCl_4$ acceptor doping concentration (N_A) on J–V curves and energy band distributions of the quasi-2D/2D structure PSCs, respectively. From a practical point of view, the $NH_3(CH_2)_2NH_3MnCl_4$ N_A varies from 3.2×10^{12} cm^{-3} to 3.2×10^{20} cm^{-3}. The V_{oc} and FF downgrade evidently with the N_A of $NH_3(CH_2)_2NH_3MnCl_4$ exceeding 3.2×10^{14} cm^{-3}. The lower V_{oc} is associated with the decrease of barrier height (non-equilibrium state) [as shown in Fig. 6(b)] caused by the heavier N_A. This is due to the heavier N_A eventuates the upward bending of the energy bands at the interface of $(BA)_2MASn_2I_7$ absorber layer and $NH_3(CH_2)_2NH_3MnCl_4$ absorber layer (the transport of electrons will be blocked), and the upward shift in the energy band curves of the $NH_3(CH_2)_2NH_3MnCl_4$ absorber layer. Additionally, this result can be interpreted from the PCE and recombination rate diagrams in Figs. 6(c) and (d), respectively. It can be definitely noticed that there is more carrier recombination when the N_A of the $NH_3(CH_2)_2NH_3MnCl_4$ absorber layer surpasses 3.2×10^{14} cm^{-3} [as shown in Fig. 6(d)]. Accordingly, more carriers will be captured by the defects, and carriers cannot be sufficiently separated and transported to the corresponding electrode. Therefore, from a practical point of view, the efficient PSCs devices (26.47%) can be yielded when the moderate N_A (3.2×10^{14} cm^{-3}) in the $NH_3(CH_2)_2NH_3MnCl_4$ absorber layer.

The proposed PSCs configurations have distinct combinations of interfacial layers to assess the device performance whilst considering the same interfacial layers doping concentration (1×10^{16} cm^{-3}). Figures 7(a) and (b) display the effects of various interfacial layers such as BiI_3, WS_2, $In_2(O, S)_3$, SnS_2, and ZnSnO on J–V characteristic curves and electric field distributions of the quasi-2D/2D structure PSCs, respectively. These interfacial layers' detailed material parameters are

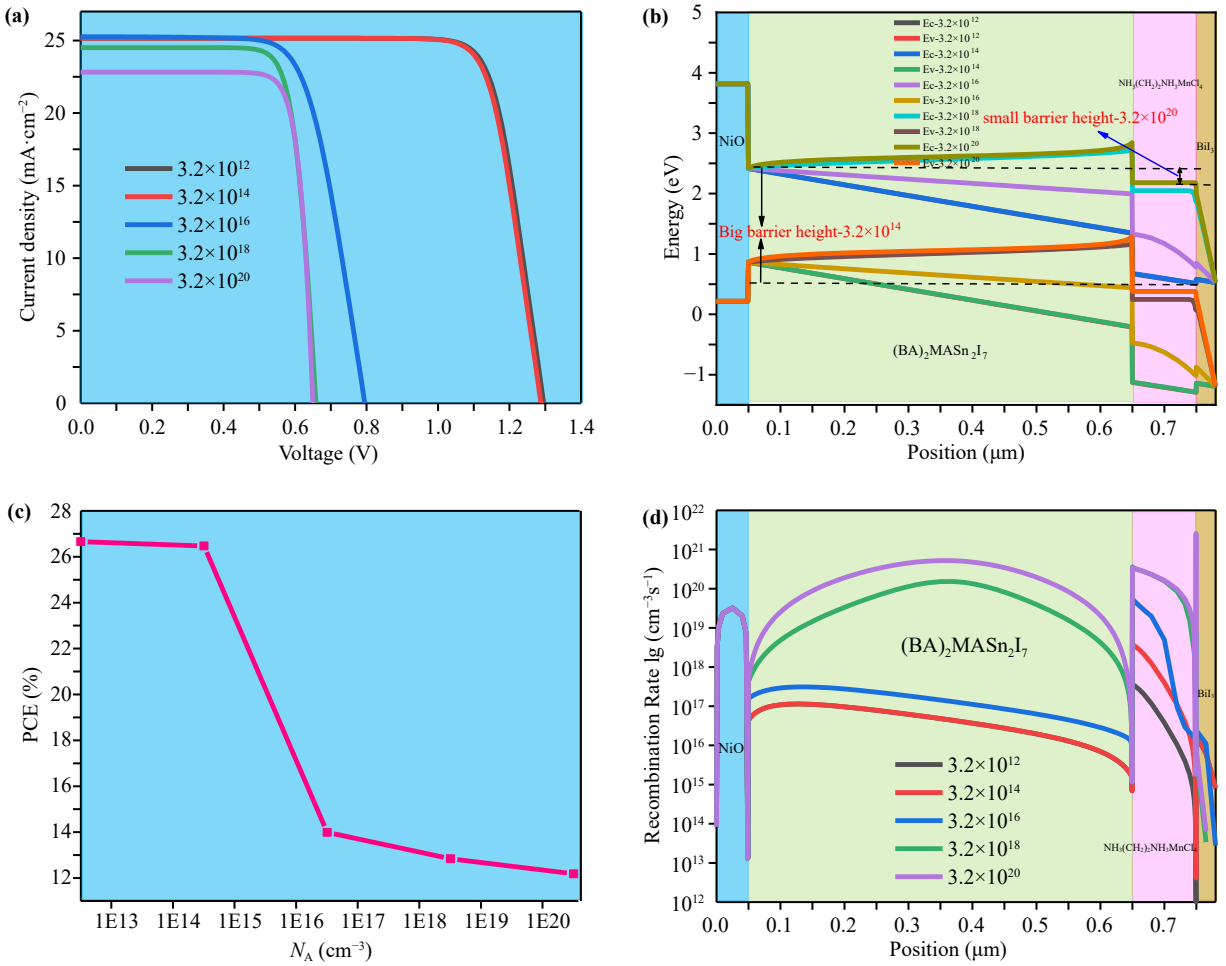

Fig. 6 Impact of acceptor doping concentration of $NH_3(CH_2)_2NH_3MnCl_4$ on **(a)** *J–V* curves, **(b)** energy band distributions, **(c)** power conversion efficiency, and **(d)** recombination rate diagrams (under the illumination condition of AM 1.5G solar spectrum and applied voltage of –0.3 V).

displayed in Table 3 [58–60]. The detailed PSCs' performance parameters for different interfacial layers are presented in Table 4. Combined with Fig. 7(a) and Table 4, the J_{sc} of the five different interfacial layers of PSCs has hardly changed. Nevertheless, the ZnSnO interfacial layer PSCs have a maximum V_{oc} (1.56 V), this is owing to the quasi-2D/2D double-layer structured solar cells similar to tandem solar cells designed by us have the potential to break through the Shockley–Queisser (S–Q) theoretical efficiency limit of single-junction solar cells. Moreover, the strongest built-in electric field near the interface of $NH_3(CH_2)_2NH_3MnCl_4/BiI_3$ (space charge region) based on ZnSnO interfacial layer PSCs [as shown in Fig. 7(b)]. The large electric field will facilitate the separation and extraction of carriers. Additionally, the WS_2 and $In_2(O, S)_3$ interfacial layers PSCs have greater FF and PCE. The series resistance (R_s) of the different interfacial layers PSCs, as exhibited in Fig. 7(c). The R_s originate from the metal contacts that interlink the PSCs and the layers that make it up [61]. The R_s is obtained by calculating the total of several resistances from every active material, each of which has its bulk resistances, including the resistance at the interface between functional layer semiconductors and metal contacts. The lower R_s and electron affinity appear at the WS_2 and $In_2(O, S)_3$ interfacial layers PSCs, thus generating superior FF and PCE. These results indicate that extracting the interfacial layer of PSCs with low series resistance can be conducive to achieving optimal device performance. Consequently, the $In_2(O, S)_3$ interfacial layer is utilized in our device configuration has derived optimal PCE (30.09%).

4 Conclusions

The computation simulation study on the novel design of inverted bilayer PSCs having the configuration FTO/NiO/quasi-2D/2D/BiI_3/Au with carrier transport mechanism has been performed for the first time by carrying out the wxAMPS simulator. The simulation

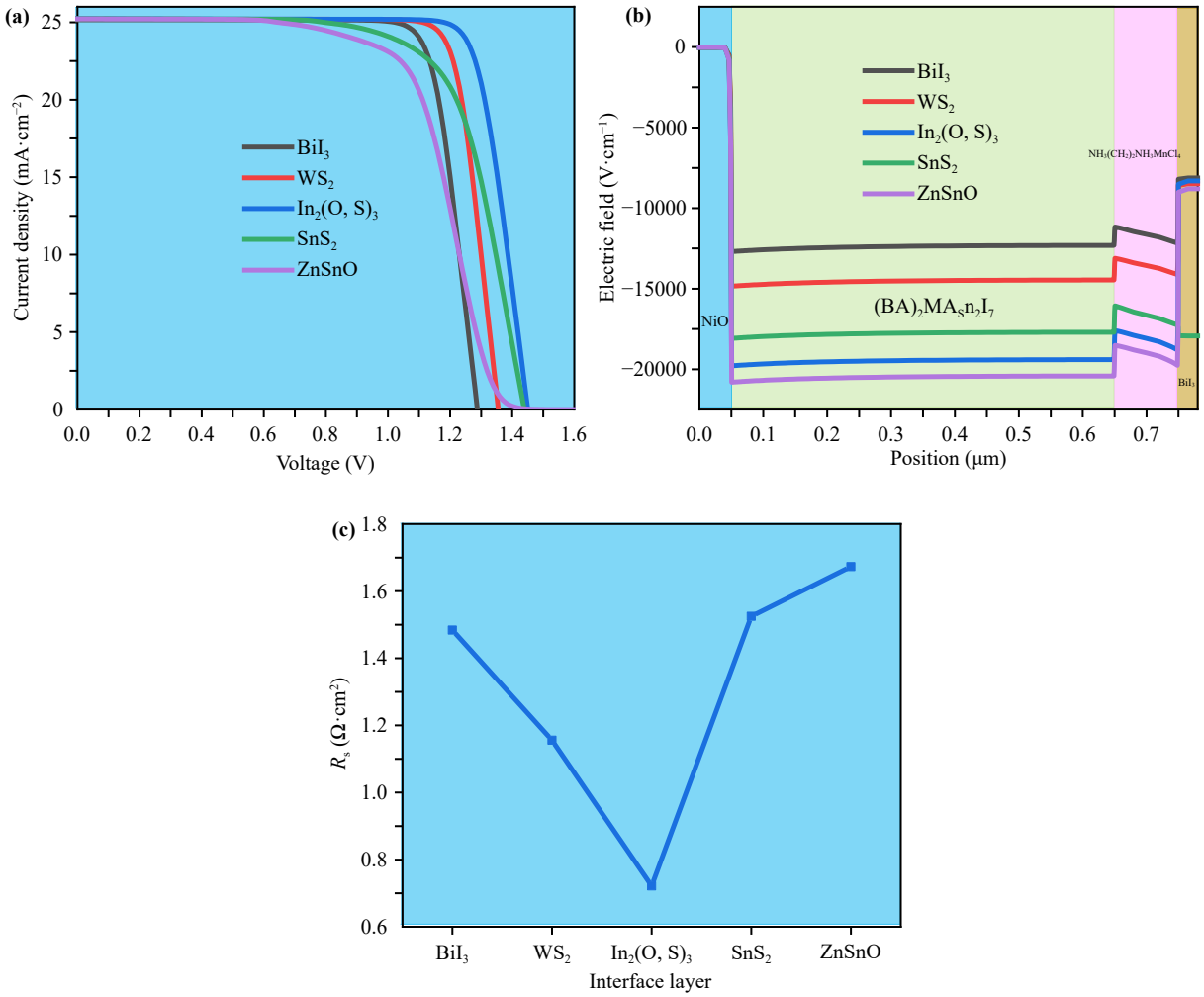

Fig. 7 **(a)** *J*–*V* characteristic curves, **(b)** electric field distributions, and **(c)** series resistance of PSCs with different interfacial layers (under the illumination condition of AM 1.5G solar spectrum and applied voltage of –0.3 V).

Table 3 Material parameters of the interfacial layers.

Parameters	WS_2 [58]	$In_2(O, S)_3$ [59]	SnS_2 [60]	ZnSnO [60]
Thickness/nm	30	30	30	30
Relative permittivity ε_r	13.6	13.5	10	9
Electron affinity χ (eV)	3.95	3.85	4.24	4.29
Band gap E_g (eV)	2.1	2.1	2.24	2.7
Effective conduction band density N_c (cm^{-3})	2×10^{18}	1.8×10^{19}	7.32×10^{18}	2.2×10^{18}
Effective valence band density N_v (cm^{-3})	2×10^{18}	4×10^{13}	1.8×10^{19}	1.8×10^{19}
Electron mobility μ_n ($cm^2\cdot V^{-1}\cdot s^{-1}$)	100	400	50	30
Hole mobility μ_p ($cm^2\cdot V^{-1}\cdot s^{-1}$)	25	210	50	5
Acceptor density N_A (cm^{-3})	1×10^{16}	1×10^{16}	1×10^{16}	1×10^{16}
Donor density N_D (cm^{-3})	1×10^{16}	1×10^{16}	1×10^{16}	1×10^{16}
Defect density N_t (cm^{-3})	1×10^{14}	1×10^{14}	1×10^{14}	1×10^{14}

revealed that the quasi-2D/2D structure can facilitate the efficient diffusion motion and transmission of charge carriers to corresponding electrode and suppress the defect state density and carrier recombination benefiting from the gentle stepped energy band structure and there's no bending of the energy band, thereby the higher FF (78.58%) and PCE (23.01%) for the proposed quasi-2D/2D structure PSCs have been achieved. Addi-

Table 4 Performance parameters of the quasi-2D/2D structure PSCs with various interfacial layers.

Parameters	V_{oc} (V)	J_{sc} (mA·cm^{-2})	FF (%)	PCE (%)
BiI_3	1.29	25.16	81.69	26.47
WS_2	1.36	25.22	83.10	28.40
$In_2(O, S)_3$	1.45	25.24	82.22	30.09
SnS_2	1.44	25.23	70.37	25.55
ZnSnO	1.56	25.22	59.43	23.42

tionally, by optimizing the thickness parameters of each absorber layer, and the doping concentration of the $NH_3(CH_2)_2NH_3MnCl_4$ absorber layer, it was demonstrated that the thickness of $(BA)_2MASn_2I_7$ has a positive influence on the J_{sc} and FF of the device, and the optimum $(BA)_2MASn_2I_7$ thickness (600 nm) can obtain high cell efficiency. Nevertheless, the thickness of $NH_3(CH_2)_2NH_3MnCl_4$ has a negative influence on the performance parameters of the device. This is attributed to the inferior carrier's diffusion length and mobility inside the 2D perovskite. The thicker $NH_3(CH_2)_2NH_3MnCl_4$ absorber layer will increase the carrier recombination probability to a large extent, and the PCE of the device will decline profoundly. Hence, the optimal PCE (24.77%) can be derived when the minor thickness (100 nm) of the $NH_3(CH_2)_2NH_3MnCl_4$ absorber layer. The performance of the device can also be effectively heightened with the moderate doping concentration (3.2×10^{14} cm^{-3}) in the $NH_3(CH_2)_2NH_3MnCl_4$ absorber layer. Lastly, the optimal-performance (30.09%) photoelectric devices can be created with the $In_2(O, S)_3$ interfacial layer PSCs of lower series resistance (R_s). This study will tender a theoretical basis for the fabrication of high-efficiency and stable PSCs.

Declarations The authors declare that they have no known competing financial interests or personal relationships that could have appeared to influence the work reported in this paper.

Data availability Data will be made available on request.

Acknowledgements This work was supported by the National Key R&D Program of China (Grant No. 2018YFA0704300) and the Natural Science Foundation of Jiangsu Province of China (Grant No. BK20201285). The authors are grateful to Dr. Yiming Liu, Prof. Angus Rockett of University of Illinois and Prof. S Fonash of the Pennsylvania State University for providing the wxAMPS program used in the simulations.

References

1. N. Droseros, D. Tsokkou, and N. Banerji, Photophysics of methylammonium lead tribromide perovskite: Free carriers, excitons, and sub-bandgap states, *Adv. Energy Mater.* 10(13), 1903258 (2020)
2. Q. Qu, J. Zhou, X. Xi, B. Wang, Z. Wan, J. Wang, H. Liu, H. Zhou, H. Wang, and S. Bi, Stable high conversion efficiency of quasi-2D perovskite solar cells via potassium iodide as additive, *Chem. Eng. J.* 466, 142999 (2023)
3. R. M. Nie, R. R. Sumukam, S. H. Reddy, M. Banavoth, and S. I. Seok, Lead-free perovskite solar cells enabled by hetero-valent substitutes, ENERG, *Energy Environ. Sci.* 13(8), 2363 (2020)
4. Y. Gan, G. Qiu, C. Yan, Z. Zeng, B. Qin, X. Bi, and Y. Liu, Numerical analysis on the effect of the conduction band offset in Dion-Jacobson perovskite solar cells, *Energies* 16(23), 7889 (2023)
5. J. Zhao, Z. Zhang, G. Li, M. H. Aldamasy, M. Li, and A. Abate, Dimensional tuning in lead-free tin halide perovskite for solar cells, *Adv. Energy Mater.* 13(13), 2204233 (2023)
6. A. Kojima, K. Teshima, Y. Shirai, and T. Miyasaka, Organometal halide perovskites as visible-light sensitizers for photovoltaic cells, *J. Am. Chem. Soc.* 131(17), 6050 (2009)
7. S. Sajid, H. Huang, J. Ji, H. Jiang, M. Duan, X. Liu, B. Liu, and M. Li, Quest for robust electron transporting materials towards efficient, hysteresis-free and stable perovskite solar cells, *Renew. Sustain. Energy Rev.* 152, 111689 (2021a)
8. Y. Zhao, F. Ma, Z. Qu, S. Yu, T. Shen, H. X. Deng, X. Chu, X. Peng, Y. Yuan, X. Zhang, and J. You, Inactive $(PbI_2)_2RbCl$ stabilizes perovskite films for efficient solar cells, *Science* 377(6605), 531 (2022)
9. C. Liu, J. Chen, and P. Gao, Enhanced perovskite photovoltaics with non-conjugated polymers: recent developments and future prospects, *ACS Appl. Polym. Mater.* 6(7), 3573 (2024)
10. Z. Liang, Y. Zhang, H. Xu, W. Chen, B. Liu, J. Zhang, H. Zhang, Z. Wang, D. H. Kang, J. Zeng, X. Gao, Q. Wang, H. Hu, H. Zhou, X. Cai, X. Tian, P. Reiss, B. Xu, T. Kirchartz, Z. Xiao, S. Dai, N. G. Park, J. Ye, and X. Pan, Homogenizing out-of-plane cation composition in perovskite solar cells, *Nature* 624(7992), 557 (2023)
11. X. Dong, X. Li, X. Wang, Y. Zhao, W. Song, F. Wang, S. Xu, Z. Miao, and Z. Wu, Improve the charge carrier transporting in two-dimensional Ruddlesden-Popper perovskite solar cells, *Adv. Mater.* 36(19), 2313056 (2024)
12. A. Kumar, S. Singh, K. Srivastava, A. Sharma, and D. K. Sharma, Performance and stability enhancement of mixed dimensional bilayer inverted perovskite $(BA_2PbI_4/MAPbI_3)$ solar cell using drift- diffusion model, *Sustain. Chem. Pharm.* 29, 100807 (2022)
13. S. Dai, H. Cao, W. Sharmoukh, Y. Qiang, L. Zhao, Y. Chen, Y. Li, H. Nasser Abdelhamid, N. Taghavinia, and

Z. Yu, Pure-phase two-dimensional perovskite capping layer enables high-performance and durable carbon-based photovoltaics, *Chem. Eng. J.* 497, 154611 (2024)
14. M. A. Karim, K. Matsuishi, T. H. Chowdhury, M. Abdel-Shakour, Y. He, and A. Islam, Additive-assisted electronic defect passivation in lead-free tin perovskite solar cells: Suppression of Sn^{2+} oxidation and I^- losses, *ACS Appl. Energy Mater.* 5(12), 15038 (2022)
15. B. P. Kore, M. Jamshidi, and J. M. Gardner, The impact of moisture on the stability and degradation of perovskites in solar cells, *Mater. Adv.* 5(6), 2200 (2024)
16. Q. Qu, J. Zhou, X. Xi, B. Wang, Z. Wan, J. Wang, H. Liu, H. Zhou, H. Wang, and S. Bi, Stable high conversion efficiency of quasi-2D perovskite solar cells via potassium iodide as additive, *Chem. Eng. J.* 466, 142999 (2023)
17. D. Kim and M. Ahmadi, Elucidating the spatial dynamics of charge carriers in quasi-two-dimensional perovskites, *ACS Appl. Mater. Interfaces* 13(29), 35133 (2021)
18. S. Luo, J. Wang, B. Yang, and Y. Yuan, Recent advances in controlling the crystallization of two-dimensional perovskites for optoelectronic device, *Front. Phys. (Beijing)* 14(5), 53401 (2019)
19. X. Liu, M. Tai, J. Gu, Z. Wu, H. Zhong, X. Wang, Z. Wang, and H. Lin, Vertically-aligned quasi-2D cesium lead halide perovskite solar cells, *J. Mater. Chem. C* 10(30), 10964 (2022)
20. F. Zheng, T. Raeber, S. Rubanov, C. Lee, A. Seeber, C. Hall, T. A. Smith, M. Gao, D. Angmo, and K. P. Ghiggino, Spontaneous formation of a ligand-based 2D capping layer on the surface of quasi-2D perovskite films, *ACS Appl. Mater. Interfaces* 14(46), 51910 (2022)
21. A. Kumar, S. Singh, M. K. A. Mohammed, and A. E. Shalan, Effect of 2D perovskite layer and multivalent defect on the performance of 3D/2D bilayered perovskite solar cells through computational simulation studies, *Sol. Energy* 223, 193 (2021)
22. J. Hu, X. Wen, and D. Li, Optical properties of two-dimensional perovskites, *Front. Phys. (Beijing)* 18(3), 33602 (2023)
23. I. C. Smith, E. T. Hoke, D. Solis-Ibarra, M. D. McGehee, and H. I. Karunadasa, A layered hybrid perovskite solar-cell absorber with enhanced moisture stability, *Angew. Chem. Int. Ed.* 53(42), 11232 (2014)
24. C. Zuo, A. Scully, W. Tan, F. Zheng, K. P. Ghiggino, D. Vak, H. Weerasinghe, C. R. McNeill, D. Angmo, A. S. R. Chesman, and M. Gao, Crystallisation control of drop-cast quasi-2D/3D perovskite layers for efficient solar cells, *Commun. Mater.* 1(1), 33 (2020)
25. B. Hailegnaw, F. Mayr, C. Putz, L. Lehner, K. Gugujonovic, S. Demchyshyn, M. Kaltenbrunner, and M. C. Scharber, The role of alpha-methylbenzyl ammonium iodide to reduce defect densities in perovskite devices, *Sol. RRL* 7(20), 2300316 (2023)
26. C. Zuo, A. D. Scully, D. Vak, W. Tan, X. Jiao, C. R. McNeill, D. Angmo, L. Ding, and M. Gao, Self-assembled 2D perovskite layers for efficient printable solar cells, *Adv. Energy Mater.* 9(4), 1803258 (2019)
27. Y. Yan, Z. Li, and Z. Lou, Photodetector based on Ruddlesden-Popper perovskite microwires with broader band detection, *J. Semicond.* 44(8), 082201 (2023)
28. W. Zhang, Z. Liu, L. Zhang, H. Wang, C. Jiang, X. Wu, C. Li, S. Yue, R. Yang, H. Zhang, J. Zhang, X. Liu, Y. Zhang, and H. Zhou, Ultrastable and efficient slight-interlayer-displacement 2D Dion-Jacobson perovskite solar cells, *Nat. Commun.* 15(1), 5709 (2024)
29. X. Li, W. Hu, Y. Shang, X. Yu, X. Wang, W. Zhou, M. Wang, Q. Luo, C. Q. Ma, Y. Lu, and S. Yang, Phenylformamidinium-enabled quasi-2D Ruddlesden-Popper perovskite solar cells with improved stability, *J. Energy Chem.* 66, 680 (2022)
30. H. Banerjee, M. K. Nazeeruddin, and S. Chakraborty, Tuning electronic and optical properties of 2D/3D Interfaces of hybrid perovskites through interfacial charge transfer: Prediction of higher-efficiency interface solar cells using hybrid-DFT methods, *ACS Appl. Mater. Interfaces* 17(13), 19701 (2025)
31. S. Cao, H. Chen, Y. Su, L. Shi, and P. Qian, What factors reduce carrier mobility of organic-inorganic hybrid perovskite for $(BA)_2MAGe_2I_7$ and $(BA)_2MASn_2I_7$, *Appl. Surf. Sci.* 546, 149075 (2021)
32. H. Wang, Y. Chen, and D. Li, Two/Quasi-two-dimensional perovskite-based heterostructures: Construction, properties and applications, *Int. J. Extreme Manuf.* 5(1), 012004 (2023)
33. O. Tahiri, S. Kassou, M. Ettakni, and A. Belaaraj, Simulation studies of lead-free Mn-based 2D perovskite solar cells, *Semicond. Sci. Technol.* 36(9), 095043 (2021)
34. N. Schopp, V. V. Brus, J. Lee, G. C. Bazan, and T. Q. Nguyen, A simple approach for unraveling optoelectronic processes in organic solar cells under short-circuit conditions, *Adv. Energy Mater.* 11(1), 2002760 (2021)
35. Q. Duan, J. Ji, X. Hong, Y. Fu, C. Wang, K. Zhou, X. Liu, H. Yang, and Z. Y. Wang, Design of hole-transport-material free $CH_3NH_3PbI_3/CsSnI_3$ all-perovskite heterojunction efficient solar cells by device simulation, *Sol. Energy* 201, 555 (2020)
36. Y. Liu, Y. Sun, and A. Rockett, A new simulation software of solar cells — wxAMPS, *Sol. Energ. Mat. Sol. C* 98, 124 (2012)
37. G. Li, M. Xu, Z. Chen, and X. Zou, Design and simulation investigations on electron transport layer-free in tin-based p-n homojunction perovskite solar cells, *Mater. Today Commun.* 35, 106232 (2023)
38. Y. Wang, Z. Xia, Y. Liu, and H. Zhou, Simulation of perovskite solar cells with inorganic hole transporting materials, in: 2015 IEEE 42nd Photovoltaic Specialist Conference (PVSC), 2015
39. N. Zibouche and M. S. Islam, Structure-electronic property relationships of 2D Ruddlesden-Popper tin-and lead-based iodide perovskites, *ACS Appl. Mater. Interfaces* 12(13), 15328 (2020)
40. K. Ahmad, W. Raza, R. A. Khan, A. Alsalme, and H. Kim, Numerical simulation of $NH_3(CH_2)_2NH_3MnCl_4$ based Pb-free perovskite solar cells via SCAPS-1D, *Nanomaterials (Basel)* 12(19), 3407 (2022)
41. S. Karthick, J. Boucle, and S. Velumani, Effect of bismuth iodide (BiI_3) interfacial layer with different HTL's in FAPI based perovskite solar cell-SCAPS-1D study, *Sol. Energy* 218, 157 (2021)
42. N. F. Coutinho, S. Cucatti, R. B. Merlo, J. M. C. Silva Filho, N. F. B. Villegas, F. Alvarez, A. F. Nogueira, and F. C. Marques, The thermomechanical properties of

thermally evaporated bismuth triiodide thin films, *Sci. Rep.* 9(1), 11785 (2019)
43. L. C. Lee, T. N. Huq, J. L. Macmanus-Driscoll, and R. L. Z. Hoye, Research update: Bismuth-based perovskite-inspired photovoltaic materials, *APL Mater.* 6(8), 84502 (2018)
44. R. E. Brandt, V. Stevanovic, D. S. Ginley, and T. Buonassisi, Identifying defect-tolerant semiconductors with high minority-carrier lifetimes: Beyond hybrid lead halide perovskites, *MRS Commun.* 5(2), 265 (2015)
45. H. Han, M. K. Hong, S. S. Gokhale, S. B. Sinnott, K. Jordan, J. E. Baciak, and J. C. Nino, Defect engineering of BiI_3 single crystals: Enhanced electrical and radiation performance for room temperature gamma-ray detection, *J. Phys. Chem. C* 118(6), 3244 (2014)
46. Z. Ni, C. Bao, Y. Liu, et al., Resolving spatial and energetic distributions of trap states in metal halide perovskite solar cells, *Science* 367, 1352 (2020)
47. K. Ahmad, W. Raza, R. A. Khan, A. Alsalme, and H. Kim, Numerical simulation of $NH_3(CH_2)_2NH_3MnCl_4$ based Pb-free perovskite solar cells via SCAPS-1D, *Nanomaterials (Basel)* 12(19), 3407 (2022)
48. X. Li, Y. Guan, X. Li, and Y. Fu, Stereochemically active lone pairs and nonlinear optical properties of two-dimensional multilayered tin and germanium iodide perovskites, *J. Am. Chem. Soc.* 144(39), 18030 (2022)
49. J. Yin, X. Zhao, M. Zhao, L. Zhang, J. Tian, Y. Wei, Z. Ma, and Y. Zhou, Effects of subcell bandgap matching on the performance of perovskite/Cu(In, Ga)Se_2 tandem solar cells, *Mater. Today Commun.* 40, 109725 (2024)
50. E. Gutierrez-Partida, M. Rusu, F. Zu, M. Raoufi, J. Diekmann, N. Tokmoldin, J. Warby, D. Menzel, F. Lang, S. Shah, S. Shoaee, L. Korte, T. Unold, N. Koch, T. Kirchartz, D. Neher, and M. Stolterfoht, Toward understanding the built-in field in perovskite solar cells through layer-by-layer surface photovoltage measurements, *ACS Appl. Mater. Interfaces* 17(7), 11176 (2025)
51. X. Zhang, H. Zhou, C. Hu, et al., Performance analysis of all-inorganic $Cs_3Sb_2I_9$ perovskite solar cells with micro-offset energy level structure by SCAPS-1D simulation and First-principles calculation, *Sol. Energ. Mat. Sol. C* 260, 112487 (2023)
52. J. Cheng, H. Cao, S. Zhang, F. Yue, and Z. Zhou, Reinforcing built-in electric field to enable efficient carrier extraction for high-performance perovskite solar cells, *Mater. Chem. Front.* 8(4), 956 (2024)
53. Y. N. Zhang, B. Li, L. Fu, Y. Zou, Q. Li, L. W. Yin, Enhanced optical absorption and efficient cascade electron extraction based on energy band alignment double absorbers perovskite solar cells, *Sol. Energ. Mat. Sol. C* 194, 168 (2019)
54. X. He, H. Chen, J. Yang, T. Wang, X. Pu, G. Feng, S. Jia, Y. Bai, Z. Zhou, Q. Cao, and X. Li, Enhancing hole transport uniformity for efficient inverted perovskite solar cells through optimizing buried interface contacts and suppressing interface recombination, *Angew. Chem. Int. Edit.* 2024, e202412601 (2024)
55. A. Hosen, S. Yeasmin, K. M. S. Bin Rahmotullah, M. F. Rahman, and S. R. A. Ahmed, Design and simulation of a highly efficient $CuBi_2O_4$ thin-film solar cell with hole transport layer, *Opt. Laser Technol.* 169, 110073 (2024)
56. A. Bag, R. Radhakrishnan, R. Nekovei, and R. Jeyakumar, Effect of absorber layer, hole transport layer thicknesses, and its doping density on the performance of perovskite solar cells by device simulation, *Sol. Energy* 196, 177 (2020)
57. H. Shen, X. Li, X. Zhang, H. Zhou, H. Zhang, X. Liu, M. Zhang, J. Wu, Z. Xiang, and W. Fang, Constructing gradient structure to increase efficiency for carbon-based hole transport layer free all-inorganic perovskite solar cells using SCAPS-1D, *Sol. Energy* 253, 240 (2023)
58. S. R. A. Ahmed, M. Rahaman, A. Sunny, S. Rahman, M. Saiful Islam, T. Abd El-Mohaymen Taha, Z. A. Alrowaili, and M. Suruz Mian, Enhancing the efficiency of Cu_2Te thin-film solar cell with WS_2 buffer layer: A simulation study, *Opt. Laser Technol.* 159, 108942 (2023)
59. E. Moradi Haghighi and A. A. Orouji, Optimizing interface energy band alignment in Cd-free Sb_2Se_3 solar cells by controlling the oxygen content of $In_2(O, S)_3$ buffer layer to improve the efficiency: A simulation study, *Opt. Laser Technol.* 169, 110107 (2024)
60. A. Kowsar, M. Shafayet-Ul-Islam, M. A. Ali Shaikh, M. L. Palash, A. Kuddus, M. I. Uddin, and S. F. U. Farhad, Enhanced photoconversion efficiency of Cu_2MnSnS_4 solar cells by Sn-/Zn-based oxides and chalcogenides buffer and electron transport layers, *Sol. Energy* 265, 112096 (2023)
61. M. K. A. Mohammed, A. K. Al-Mousoi, A. Kumar, M. M. Sabugaa, R. Seemaladinne, R. Pandey, J. Madan, M. K. Hossain, B. S. Goud, and A. A. Al-Kahtani, Harnessing the potential of Dion-Jacobson perovskite solar cells: Insights from SCAPS simulation techniques, *J. Alloys Compd.* 963, 171246 (2023)